IEEE Access
Multidisciplinary | Rapid Review | Open Access Journal

Received March 11, 2020, accepted March 24, 2020, date of publication April 3, 2020, date of current version April 20, 2020.

Digital Object Identifier 10.1109/ACCESS.2020.2985380

Fractional-Order Adaptive Integral Hierarchical Sliding Mode Control Method for High-Speed Linear Motion of Spherical Robot

LONG MA, HANXU SUN, AND JINGZHOU SONG, (Member, IEEE)
School of Automation, Beijing University of Posts and Telecommunications, Beijing 100876, China

Corresponding author: Jingzhou Song (sxml_444647811@ 126.com)

This work was supported in part by the National Natural Science Foundation of China under Grant 51175048, in part by the Fundamental Research Funds for the Central Universities under Grant 2019XD-A16, and in part by the Special Basic Scientific Research Foundation of Central Universities under Grant 2018RC57.

ABSTRACT The development of the spherical robot to meet the requirements of high-speed and high-precision tasks is of great importance. In this study, a fractional-order adaptive integral hierarchical sliding mode controller (F-AIHSMC) is proposed. F-AIHSMC enables the spherical robot to have better controlled performance when facing unknown disturbances and system chattering, which can seriously affect the high-speed and high-precision motion of the spherical robot. We establish the standard dynamic model of the spherical robot for high-speed linear motion first, and then use the feedforward compensation method to compensate the controllable influencing factors in the motion process. According to the standard dynamic model, the integral term and fractional calculus methods are integrated into the hierarchical sliding mode controller, and the adaptive method is used to evaluate and compensate unknown disturbances in the high-speed motion process. In order to verify the efficiency of the proposed F-AIHSMC, we test its control effect using the BYQ-GS spherical robot. The experimental results demonstrate that, compared with the classical hierarchical sliding mode controller and the adaptive hierarchical sliding mode controller, the F-AIHSMC has obvious advantages in response speed, convergence speed, stability and robustness when being applied to the control of high-speed linear motion of spherical robot. Moreover, the advantages of its control performance are more highlighted with the increase of the speed of the spherical robot.

INDEX TERMS Adaptive control, fractional calculus, hierarchical sliding mode control, high-speed motion control, spherical robot.

I. INTRODUCTION

The spherical robot is a new type of mobile robot that moves based on the eccentric torque and inertial force generated by the internal drive mechanism. Compared with the traditional mobile robot, the spherical robot has the spherical closed shell, which enables the robot to have the ability of overturn-preventing, stable and rapid omnidirectional motion, while protecting the internal unit from interference and damage of terrain and road. The point contact between the sphere and ground makes the spherical robot have the advantages of high motion efficiency and low energy consumption, which make the robot have a broad application prospect in the fields of hazardous environment detection, narrow space operation, monitoring and reconnaissance [1]–[3]. The spherical robot system has the characteristics of strong coupling, under-actuation, non-holonomic constraints and nonlinearity. Therefore, it cannot be effectively controlled by conventional motion control methods. At the same time, there are unmeasurable and unstable factors in the process of motion, such as incomplete dynamic model construction and unknown disturbances from the surrounding environment to the motion [4], [5]. With gradual increase of the motion speed, the influence of the above unstable factors on the motion control of the spherical robot increases rapidly. Meanwhile, the motion accuracy is greatly reduced, which makes the spherical robot unable to cope with tasks requiring high-speed motion ability, such as military reconnaissance

The associate editor coordinating the review of this manuscript and approving it for publication was Zhong Wu.

blasting, communication network relay, and so on. Therefore, it is of great significance to study the control method for high-speed and high-precision motion of the spherical robot.

In recent years, the driving mechanism of the spherical robot that experts and scholars concentrate on is mainly divided into the following three types: eccentric torque driving mechanism based on omnidirectional wheel, internal driving mechanism based on friction and eccentric torque driving mechanism based on weight pendulum. Relevant studies mainly focus on the control strategy of low-speed motion (for a small robot of about 20kg, the definition standard of high-speed is 2.5m/s) [6]. The studies on the control strategy of spherical robot in high-speed motion are few. Compared with the other two kinds of driving mechanism, the eccentric torque driving mechanism based on weight pendulum is a driving mechanism with higher maneuverability and easier implementation. However, in the process of motion, the strong coupling and under-actuation between the shell and the weight pendulum are the reasons for high control difficulty of the spherical robot. Even so, the spherical robot using this drive mechanism still has obvious advantages in the speed of motion. Therefore, we study the control method for the linear motion of the spherical robot under high-speed motion state using the spherical robot driven by the eccentric torque driving mechanism based on weight pendulum.

In practical applications, the internal frame of the spherical robot needs to be equipped with corresponding equipments and instruments. Therefore, in the process of motion, it is equally important to keep the stability of the spherical shell as well as the inner mechanism. As a typical under-actuated system, the spherical robot driven by the eccentric torque driving mechanism based on weight pendulum needs to face both internal and external disturbances during actual movement, which make the control of the spherical robot much more complicated. Sliding mode control (SMC), which is widely used in the field of robot control, has the ability to overcome the uncertainty of the system and has strong robustness to unknown disturbances, especially has good effect on the control of nonlinear system [7]–[10]. The hierarchical sliding mode control (HSMC) based on SMC can construct the first layer sliding surfaces for each state variable, and then construct the second layer sliding surface by combining the first layer sliding surfaces. HSMC not only retains the advantages of SMC, but also has the ability to control different outputs simultaneously. Because of the above advantages, HSMC is widely used in the study of the spherical robot.

The latest studies on HSMC focus on the strategies to improve the robustness facing unknown disturbances. [11]–[16] adopt quite complicated methods, such as radial basis function networks, self-recurrent wavelet neural networks, and the method of combining fuzzy control with adaptive control, to cope with the impact of unknown disturbances on the control accuracy. In practical applications, these methods are mainly used in the situation of low speed and low real-time requirements, such as the control of overhead crane, the attitude regulation control of satellite, and the control of low-speed mobile robot. The verification approaches of most of these studies are only simulation results.

There are a lot of studies on the linear motion control method of the spherical robot. Some studies focus on the motion model, such as the speed and angle controller based on linear quadratic regulator (LQR) for the linear motion of the spherical robot. The linearization of linear motion model makes the accuracy of this control method difficult to guarantee [17]. Some studies incorporate feedback control to ensure robustness of the spherical robot to constant disturbance, but these control methods are neither robust against nor adaptive to external unpredictable time-varying disturbances [18], [19]. It is an vital direction to realize the linear motion of the spherical robot using the control methods based on HSMC. These control methods can obtain relatively ideal control effect by using the fuzzy reasoning method or the real-time estimation of rolling friction, except that the overshoot is large [20]–[22]. Another very popular robust control method for linear motion control of the spherical robot is based on fractional calculus control techniques. Fractional calculus is an arbitrary order of ordinary derivatives and integrals. The application of fractional calculus can help eliminate external interference and steady-state error, improve convergence speed and trajectory tracking performance of the spherical robot during linear motion [23], [24]. Some studies use the control method that incorporates fractional calculus, but the adaptivity of this control method is not considered, and only simulation results are given [25].

According to the publications of linear motion control method of the spherical robot, most of the studies adopt the idealized or linearized dynamic model for linear motion of the spherical robot. Even if fuzzy or adaptive control methods are incorporated in HSMC to deal with the uncertain factors that cannot be described by sensor or mathematical model, the control law still faces the problem of excessive overshoot, poor finite convergence, and severe chattering. However, due to the low-speed of the spherical robot, the impact of the problems above on the linear motion accuracy is not obvious. For the spherical robot with high-speed and real-time requirement, the impact of a large number of uncertain factors in the actual motion environment and the impact of the defects of the control method in the state of low-speed motion on the precise and stable motion of the spherical robot will amplify rapidly, which makes it difficult for the above controllers to achieve the expected motion accuracy. Therefore, we should improve HSMC's performance by improving the basic principle of it, instead of concentrate on the complex anti-interference strategy only. Also, we should perform practicality experiment using the spherical robot, instead of the simulation method, to demonstrate the effectiveness of the control method.

Here, we propose a fractional-order adaptive integral hierarchical sliding mode controller (F-AIHSMC). Basing on the control advantages of HSMC, we introduce feedforward compensation, integral term, fractional calculus and

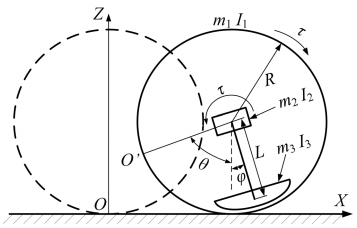

FIGURE 1. Simplified model of linear motion of the spherical robot.

corresponding adaptive law to the new method. Thus, high-precision motion control with high system response speed, finite time convergence, strong robustness and the ability to restrain chattering effectively, can be obtained. In this way, precise and stable linear motion of the spherical robot under high-speed motion can be achieved.

The rest of this study is organized as follows: Section II establishes the standard dynamic model of linear motion of the spherical robot. Section III derives the F-AIHSMC in detail. Section IV performs practicality experiments using the BYQ-GS spherical robot, to verify the effectiveness of the F-AIHSMC. Section V summarizes the results and discusses future research directions.

II. THE STANDARD DYNAMIC MODEL OF LINEAR MOTION OF THE SPHERICAL ROBOT

There are two ways of linear motion of the spherical robot using the eccentric torque driving mechanism based on weight pendulum. When the long axis motor outputs the torque alone, the spherical robot moves linearly along the X-axis direction; when the short axis motor outputs the torque alone, the spherical robot moves linearly along the Y-axis direction. Here, we take the linear motion along the X-axis as example. The simplified model of linear motion of the spherical robot is shown in Fig.1. The spherical robot moves along the X-axis in the XOZ plane under the action of the theoretical output torque τ of the long axis motor. The mass and the moment of inertia of the spherical shell are m_1 and I_1, respectively. The mass and the moment of inertia of the main frame are m_2 and I_2, respectively. The mass and the moment of inertia of the weight pendulum are m_3 and I_3, respectively. The radius of the spherical shell is R, the pendulum arm length (the distance between the gravity center of the weight pendulum and the center of the spherical shell) is L, the roll angle of the spherical shell from the initial position is θ, the displacement of the spherical center along the X-axis direction is x, and $x = \theta R$, the swing angle of the weight pendulum from vertical direction is φ, the total mass of the spherical robot is M, and $M = m_1 + m_2 + m_3$.

Based on the Lagrange method, the ideal dynamic model of linear motion of the spherical robot is built as follows [26].

$$\boldsymbol{M}(\boldsymbol{q})\ddot{\boldsymbol{q}} + \boldsymbol{N}(\boldsymbol{q}, \dot{\boldsymbol{q}}) = \boldsymbol{\tau} \tag{1}$$

where $\boldsymbol{M}(\boldsymbol{q})$ is the inertia matrix, $\boldsymbol{N}(\boldsymbol{q}, \dot{q})$ is the nonlinear term, and

$$\boldsymbol{M}(\boldsymbol{q}) = \begin{bmatrix} MR + \dfrac{I_1}{R} & m_3RL\cos\varphi \\ m_3L\cos\varphi & m_3L^2 + I_2 + I_3 \end{bmatrix}$$

$$\boldsymbol{N}(\boldsymbol{q})\dot{\boldsymbol{q}} = \begin{bmatrix} -m_3RL\sin\varphi\dot{\varphi}^2 \\ 2m_3gL\sin\varphi \end{bmatrix} \quad \boldsymbol{q} = \begin{bmatrix} x \\ \varphi \end{bmatrix} \quad \boldsymbol{\tau} = \begin{bmatrix} \tau \\ \tau \end{bmatrix}$$

According to the dynamic model shown in (1), the nonholonomic constraints on the spherical robot in linear motion are as follows.

$$h_1(\varphi)\ddot{x} + h_2(\varphi)\ddot{\varphi} - h_3(\varphi, \dot{\varphi}) = 0 \tag{2}$$

where

$$\begin{aligned} h_1(\varphi) &= MR + \frac{I_1}{R} - m_3L\cos\varphi \\ h_2(\varphi) &= m_3RL\cos\varphi - (m_3L^2 + I_2 + I_3) \\ h_3(\varphi, \dot{\varphi}) &= -m_3RL\sin\varphi\dot{\varphi}^2 - 2m_3gL\sin\varphi \end{aligned}$$

Most of studies on the spherical robot are based on the ideal dynamic model shown above. In practical application, the spherical robot needs to face many complicated friction problems and external disturbances. Friction and disturbances can produce many unknown quantities, which complicate the dynamic model of the spherical robot, especially for the spherical robot in high-speed motion. Therefore, we establish the standard dynamic model of the spherical robot as follows.

$$\boldsymbol{M}(\boldsymbol{q})\ddot{\boldsymbol{q}} + \boldsymbol{N}(\boldsymbol{q}, \dot{\boldsymbol{q}}) = \boldsymbol{\tau_m} = \tau + \tau_f + \boldsymbol{\tau_d} \tag{3}$$

where $\boldsymbol{\tau_m}$ is the output torque of the motor, $\boldsymbol{\tau_f}$ is the friction term in the motion process, and $\boldsymbol{\tau_d}$ is the external disturbance in the motion process.

Basing on whether the disturbance is controllable, we divide the disturbance $\boldsymbol{\tau_d}$ into controllable disturbance $\boldsymbol{\tau_{dv}}$ and uncontrollable disturbance $\boldsymbol{\tau_{du}}$. Also, we divide the friction term $\boldsymbol{\tau_f}$ into linear $\boldsymbol{\tau_{fx}}$ and nonlinear $\boldsymbol{\tau_{fn}}$. Therefore, the standard dynamic model is as follows.

$$\boldsymbol{M}(\boldsymbol{q})\ddot{\boldsymbol{q}} + \boldsymbol{N}(\boldsymbol{q}, \dot{\boldsymbol{q}}) = \boldsymbol{\tau} + \boldsymbol{\tau_{fx}} + \boldsymbol{\tau_{fn}} + \boldsymbol{\tau_{dv}} + \boldsymbol{\tau_{du}} \tag{4}$$

In high-speed motion, the controllable disturbance $\boldsymbol{\tau_{dv}}$, which has great influence on the precise motion of the spherical robot, mainly comes from the rolling friction couple moment applied by the ground. According to the law of rolling friction couple moment, the rolling friction couple moment of the spherical robot in the motion process can be expressed as follows [27].

$$\tau_r = -\delta F_N sign\left(\frac{\dot{x}}{R}\right) \tag{5}$$

where δ is the coefficient of rolling friction, $\dot{x}$ is the velocity of the spherical shell, F_N is the positive pressure generated by the spherical robot on the supporting surface, and the expression of F_N is

$$F_N = Mg + m_3L\dot{\varphi}^2\cos\varphi + m_3L\ddot{\varphi}^2\sin\varphi \tag{6}$$

The high-speed motion state makes the friction of spherical robot more complicated. During the linear motion of the high-speed spherical robot, the weight pendulum rotates relative to the spherical shell. The frictional moment τ_c, which is generated in the rotating joint due to the viscous damping of the bearing, is the main source of linear friction. The value of τ_c is directly proportional to the rotational speed of the joint, and the direction of τ_c is opposite to the rotational direction of the joint, and the expression is shown in (7) [27].

$$\tau_c = -\varsigma(\dot{\theta} + \dot{\varphi}) \tag{7}$$

where ς is the viscous friction coefficient.

According to the rolling friction couple moment model and the joint viscous friction model shown in (5) and (7), the expression of the controllable compensation torque τ_{fc} is

$$\boldsymbol{\tau_{fc}} = \boldsymbol{\tau_{fx}} + \boldsymbol{\tau}_{dv} = \boldsymbol{\tau_r} + \boldsymbol{\tau}_c = \tilde{\boldsymbol{M}}(\boldsymbol{q}, \dot{\boldsymbol{q}})\ddot{\boldsymbol{q}} + \tilde{\boldsymbol{N}}(\boldsymbol{q}, \dot{\boldsymbol{q}}) \tag{8}$$

where

$$\tilde{\boldsymbol{M}} = \begin{bmatrix} 0 & -\delta m_3 L \sin\varphi sign\left(\frac{\dot{x}}{R}\right) \\ 0 & 0 \end{bmatrix}$$

$$\tilde{\boldsymbol{N}} = \begin{bmatrix} -\varsigma\left(\frac{\dot{x}}{R} + \dot{\varphi}\right) - \delta M g sign\left(\frac{\dot{x}}{R}\right) - \delta m_3 L\dot{\varphi}^2 sign\left(\frac{\dot{x}}{R}\right)\cos\varphi \\ -\varsigma\left(\frac{\dot{x}}{R} + \dot{\varphi}\right) \end{bmatrix}$$

Let $\boldsymbol{\tau}_i$ denote the uncertain factors such as nonlinear friction $\boldsymbol{\tau_{fn}}$ and uncontrollable disturbance $\boldsymbol{\tau_{du}}$, the standard dynamic model of the spherical robot can be expressed as

$$\boldsymbol{M}(\boldsymbol{q})\ddot{\boldsymbol{q}} + \boldsymbol{N}(\boldsymbol{q}, \dot{\boldsymbol{q}}) = \boldsymbol{\tau} + \boldsymbol{\tau_{fc}} + \boldsymbol{\tau_i} \tag{9}$$

According to (9), when designing a spherical robot controller for high-speed motion, we need to consider the following important factors comprehensively: parameters related to the spherical robot itself, controllable factors during high-speed motion, and uncertainty factors during high-speed motion.

Let $\boldsymbol{\xi}(\boldsymbol{t}, \boldsymbol{u}(\boldsymbol{t}))$ denote the uncertainty term including the uncertain factors such as uncontrollable bounded unknown disturbance and nonlinear friction. The standard dynamic model of linear motion of the spherical robot (9) can be transformed into (10), and it can be further expressed as a state space expression of two subsystems shown in (11).

$$\begin{aligned} \ddot{\boldsymbol{q}} &= \boldsymbol{f}(\boldsymbol{q}, \dot{\boldsymbol{q}}, \boldsymbol{t}) + \boldsymbol{g}(\boldsymbol{q}, \boldsymbol{t})\boldsymbol{u}(\boldsymbol{t}) + \boldsymbol{\xi}(\boldsymbol{t}, \boldsymbol{u}(\boldsymbol{t})) \\ \boldsymbol{y} &= \boldsymbol{q} \end{aligned} \tag{10}$$

$$\begin{aligned} \ddot{q}_1 &= f_1 + g_1 u_1 + \xi_1 \\ y_1 &= q_1 \\ \ddot{q}_2 &= f_2 + g_2 u_2 + \xi_2 \\ y_2 &= q_2 \end{aligned} \tag{11}$$

where

$$\begin{aligned} \boldsymbol{f}(\boldsymbol{q}, \dot{\boldsymbol{q}}, \boldsymbol{t}) &= (f_1 \quad f_2)^T = -\boldsymbol{M}(\boldsymbol{q})^{-1}\boldsymbol{N}(\boldsymbol{q}, \dot{\boldsymbol{q}}) \\ \boldsymbol{g}(\boldsymbol{q}, \boldsymbol{t}) &= (g_1 \quad g_2)^T = \boldsymbol{M}(\boldsymbol{q})^{-1} \\ \boldsymbol{u}(\boldsymbol{t}) &= (u_1 \quad u_2)^T = \boldsymbol{\tau} + \boldsymbol{\tau_{fc}} \\ \boldsymbol{\xi}(\boldsymbol{t}, \boldsymbol{u}(\boldsymbol{t})) &= (\xi_1 \quad \xi_2)^T \end{aligned}$$

We can obtain the explicit expression for the input-output by the second derivative of the output fuction $\boldsymbol{y}$, as shown in (12).

$$\ddot{\boldsymbol{y}} = \boldsymbol{f} + \boldsymbol{g}\boldsymbol{u} + \boldsymbol{\xi} \tag{12}$$

Since the system is composed of two second-order subsystems, the relative degree r of each subsystem is 2 [28], and the relative degree of each subsystem is equal to the order of the subsystem. Therefore, the system does not contain unobservable parts. There is no zero dynamics in the system.

When the spherical robot is in dynamic equilibrium state, the balance angle of the weight pendulum will be affected by the rolling friction couple moment that the spherical robot is subjected to during the motion process. This problem cannot be ignored in the design of the controller. Otherwise, the precise control of the spherical robot cannot be achieved. According to the description of the balance angle of the weight pendulum in [29], the balance angle of the weight pendulum in equilibrium state can be determined by

$$\varphi_d = \frac{\tau_r}{m_3 g L} \tag{13}$$

The purpose of the control method proposed in our study is to design a reasonable motor output torque control law, so that the trajectory of the spherical robot $x(t)$ and the swing position of the weight pendulum $\varphi(t)$ can converge to their expected values $x_d(t)$ and $\varphi_d(t)$ in high-speed motion state, respectively, and the error of the motion trajectory $e_x(t) = x_d(t) - x(t)$ and the error of swing position of the weight pendulum $e_\varphi(t) = \varphi_d(t) - \varphi(t)$ can be as small as possible. In this case, precise linear motion of the spherical robot in high-speed motion state can be achieved.

III. FRACTIONAL-ORDER ADAPTIVE INTEGRAL HIERARCHICAL SLIDING MODE CONTROLLER (F-AIHSMC)

Facing the precise control problem of the spherical robot system in high-speed linear motion state, we introduce the idea of feedforward control. That is, when the torque $\boldsymbol{\tau}$ in ideal state acts on the spherical robot system, we use the influencing factor $\boldsymbol{\tau_{fc}}$, which has an approximate accurate model, to compensate the high-speed motion control system in advance. Using this strategy, we can reduce the influence of the system hysteresis on the high-speed motion accuracy, reduce the motion error of the spherical robot, and improve the dynamic characteristics of the system.

A. PRELIMINARIES OF FRACTIONAL CALCULUS

There are four commonly used definitions of fractional calculus: Grunwald-Letnikov fractional derivative (G-L), Riemann-Liouville fractional derivative (R-L), Caputo fractional derivative and Riesz fractional derivative. Among the four types of fractional calculus, R-L is the easiest to operate and is the most widely used definition. Its definition is shown below [30].

Definition: Define operator $\mathcal{D} = d/dt$ as $\mathcal{D}^\alpha$, where $\alpha \in \mathcal{R}$ and $n-1 \le \alpha \le n$ (n is an integer). If $\alpha > 0$, $\mathcal{D}^\alpha$ represents differential operation; if $\alpha < 0$, $\mathcal{D}^\alpha$ represents integral operation.

For the function $f(t)$, its α-order differentiation and integration with respect to t are

$$\begin{aligned}\mathcal{D}^\alpha f(t) &= \frac{d^\alpha f(t)}{dt^\alpha} = \frac{1}{\Gamma(n-\alpha)}\left(\frac{d^n}{dt^n}\right)\int_0^t \frac{f(\tau)}{(t-\tau)^{\alpha+1-n}}d\tau \\ \mathcal{D}^{-\alpha} f(t) &= \mathcal{L}^\alpha f(t) = \frac{1}{\Gamma(\alpha)}\int_0^t \frac{f(\tau)}{(t-\tau)^{1-\alpha}}d\tau \end{aligned} \tag{14}$$

where $\mathcal{D}^\alpha$ and $\mathcal{L}^\alpha$ represent fractional differential and fractional integral, respectively. $\Gamma(\cdot)$ is Euler's Gamma function, and the expression of which is

$$\Gamma(\alpha) = \int_0^\infty e^{-t}t^{\alpha-1}dt \tag{15}$$

In our study, an important property of fractional calculus is applied, and the expressions are as follows.

$$\frac{d^n}{dt^n}(\mathcal{D}^\alpha f(t)) = \mathcal{D}^\alpha\left(\frac{d^n f(t)}{dt^n}\right) = \mathcal{D}^{\alpha+n} f(t) \tag{16}$$

The discretization of fractional calculus operator is the main implementation method of fractional order controller in practicality experiment. We adopt the Al-Alaoui+CFE method proposed in [31]. In the calculation process, the fractional order operator is discretized into an approximate form, as shown in (17).

$$\begin{aligned}\mathcal{D}^\alpha\{s\} &= (8/7T)^\alpha CFE\left\{\left(\frac{1-s^{-1}}{1+s^{-1}/7}\right)^\alpha\right\}_{p,q} \\ &= (8/7T)^\alpha P_p(s^{-1})/Q_q(s^{-1})\end{aligned} \tag{17}$$

where T is the sampling period, $CFE\{u\}$ is the continued fraction expansion, $P_p(\cdot)$ and $Q_q(\cdot)$ are the relatively prime polynomials of the variable s^{-1}. Generally, the order P of $P_p(\cdot)$ and the order Q of $Q_q(\cdot)$ are equal to the iteration number n.

The iteration number n we select is 3. According to Table 3-2 in [31], we select the following expressions.

$$\begin{aligned}P_p(s^{-1}) &= (-288\alpha^2+27)s^{-3} + (-64\alpha^3-284\alpha)s^{-3} \\ &\quad + (672\alpha^2+1827)s^{-2} + 2520\alpha s^{-2} \\ &\quad - 2940\alpha s^{-1} - 6615s^{-1} + 5145 \\ Q_q(s^{-1}) &= (-288\alpha^2+27)s^{-3} - (-64\alpha^3-284\alpha)s^{-3} \\ &\quad + (672\alpha^2+1827)s^{-2} - 2520\alpha s^{-2} \\ &\quad + 2940\alpha s^{-1} - 6615s^{-1} + 5145\end{aligned} \tag{18}$$

B. THE FIRST LAYER SLIDING SURFACE WITH INTEGRAL TERM AND FRACTIONAL CALCULUS OPERATOR

Compared with the traditional SMC, the integral sliding mode controller (ISMC) can improve the response speed and robustness of the control system by introducing the integral term. Basing on the standard dynamics model of the spherical robot, we propose the design of integral hierarchical sliding mode controller (IHSMC) by combining ISMC with HSMC.

In order to ensure the asymptotic stability of the control system and the accessibility of the second layer sliding surface, the total control law of HSMC needs to include the sliding control law derived from the first layer sliding surface and the approach control law of the second layer sliding surface [32]. Therefore, the control law of IHSMC is divided into two parts:

$$u(t) = u_e(t) + u_{sw}(t) \tag{19}$$

where $u_e(t)$ is the sliding control law, which can be obtained through the first layer sliding surface of the system; $u_{sw}(t)$ is the approach control law.

Since the dynamic equations of the two subsystems of the spherical robot are both second-order nonlinear functions, we integrate the integral operator into the first layer sliding surface. Considering that the integral term can accelerate the response of the system, but meanwhile, it can also increase the overshoot of the system response, we add differential term to reduce the overshoot of the system. We design the first layer sliding surfaces $S_1(t)$ and $S_2(t)$ for the spherical shell displacement and the swinging angle of weight pendulum, respectively. The expressions are as follows [33], [34].

$$\begin{aligned}S_1(t) &= \dot{e}_x(t) + 2k_1 e_x(t) + k_1^2\int e_x(t) \\ S_2(t) &= \dot{e}_\varphi(t) + 2k_2 e_\varphi(t) + k_2^2\int e_\varphi(t)\end{aligned} \tag{20}$$

where $k_1 > 0$ and $k_2 > 0$. We can control the first layer sliding surfaces by k_1 and k_2, respectively.

Slow response speed of the controller can lead to poor stability of control. In order to make the linear motion controller of the spherical robot have high system response speed, fast terminal convergence and precise control performance, we integrate the R-L fractional calculus operator into the first layer sliding surfaces of the IHSMC, and the first layer sliding surfaces of the F-AIHSMC are designed as

$$\begin{aligned}S_1(t) &= \mathcal{D}^\alpha\{e_x(t)\} + 2k_1 e_x(t) + k_1^2\mathcal{D}^{-\alpha}\{e_x(t)\} \\ S_2(t) &= \mathcal{D}^\alpha\{e_\varphi(t)\} + 2k_2 e_\varphi(t) + k_2^2\mathcal{D}^{-\alpha}\{e_\varphi(t)\}\end{aligned} \tag{21}$$

By using the fractional calculus properties and the second-order sliding mode control theory, we calculate two derivatives of (21) with respect to time. $\ddot{S}_1(t)$ and $\ddot{S}_2(t)$ can be obtained as follows [30].

$$\begin{aligned}\ddot{S}_1 &= \mathcal{D}^{\alpha+2}\{e_x(t)\} + 2k_1\ddot{e}_x(t) + k_1^2\mathcal{D}^{2-\alpha}\{e_x(t)\} \\ \ddot{S}_2 &= \mathcal{D}^{\alpha+2}\{e_\varphi(t)\} + 2k_2\ddot{e}_\varphi(t) + k_2^2\mathcal{D}^{2-\alpha}\{e_\varphi(t)\}\end{aligned} \tag{22}$$

Let the expected value of the control target $\boldsymbol{q_d} = (x_d \;\; \varphi_d)^T$, we bring (11) into (22), and (22) can be further expressed as

$$\begin{aligned}\ddot{S}_1 &= \mathcal{D}^{\alpha+2}\{e_x(t)\} \\ &\quad + 2k_1(\ddot{x}_d - f_1 - g_1 u_{e1} - \xi_1) + k_1^2\mathcal{D}^{2-\alpha}\{e_x(t)\} \\ \ddot{S}_2 &= \mathcal{D}^{\alpha+2}\{e_\varphi(t)\} \\ &\quad + 2k_2(\ddot{\varphi}_d - f_2 - g_2 u_{e2} - \xi_2) + k_2^2\mathcal{D}^{2-\alpha}\{e_\varphi(t)\}\end{aligned} \tag{23}$$

For the second-order sliding mode control, if the sliding surface and its first and second derivatives are equal to 0, the motion error can converge to 0. Therefore, let $\dot{S}_1 = 0$ and $\ddot{S}_2 = 0$, we can get the control laws of two subsystems, as shown in (24).

$$\begin{aligned} u_{e1} &= g_1^{-1}\left[\ddot{x}_d + \frac{1}{2k_1}\mathcal{D}^{\alpha+2}\{e_x(t)\} \right. \\ &\quad \left. + \frac{k_1}{2}\mathcal{D}^{2-\alpha}\{e_x(t)\} - f_1 - \xi_1\right] \\ u_{e2} &= g_2^{-1}\left[\ddot{\varphi}_d + \frac{1}{2k_2}\mathcal{D}^{\alpha+2}\{e_\varphi(t)\} \right. \\ &\quad \left. + \frac{k_2}{2}\mathcal{D}^{2-\alpha}\{e_\varphi(t)\} - f_2 - \xi_2\right] \end{aligned} \tag{24}$$

C. THE FIRST LAYER SLIDING SURFACE WITH ADAPTIVE COMPENSATION

In the high-speed linear motion process of the spherical robot, factors that cannot be identified and measured, such as nonlinear friction and uncontrollable disturbances, need to be considered. The uncertainties ξ_1 and ξ_2 in the subsystems are essentially unknown functions with physical boundary. According to the standard dynamic model shown in (11), the unknown disturbances can act on two subsystems respectively, and generate errors in the first layer sliding surfaces. In order to restrain the errors in the first layer sliding surfaces effectively, we need to integrate the adaptive feedback control into the subsystem control laws to offset the influence of unknown disturbances. In this way, the robustness of the system can be enhanced. According to the principle of ISMC, each subsystem control law u_{ei} shown in (24) can only make the subsystem reach the first layer sliding surface. We add the stable control law u_{ei-s} as a feedback control part to the subsystem control law, by which we can improve the robustness of the spherical robot system to unknown disturbance and chattering in the high-speed linear motion process on the level of subsystem. The control law of the subsystem u_{ei} is updated to the following forms.

$$\begin{aligned} u_{e1} &= g_1^{-1}\left[\ddot{x}_d + \frac{1}{2k_1}\mathcal{D}^{\alpha+2}\{e_x(t)\} \right. \\ &\quad \left. + \frac{k_1}{2}\mathcal{D}^{2-\alpha}\{e_x(t)\} - f_1 - \xi_1\right] + u_{e1-s}(t) \\ u_{e2} &= g_2^{-1}\left[\ddot{\varphi}_d + \frac{1}{2k_2}\mathcal{D}^{\alpha+2}\{e_\varphi(t)\} \right. \\ &\quad \left. + \frac{k_2}{2}\mathcal{D}^{2-\alpha}\{e_\varphi(t)\} - f_2 - \xi_2\right] + u_{e2-s}(t) \end{aligned} \tag{25}$$

For the stable control law $u_{ei-s}(t)$ in the subsystem control law, we select the following expression

$$u_{ei-s}(t) = g_i(t)^{-1}(\mu_i sign(\dot{S}_i) + \eta_i S_i) \tag{26}$$

where μ_i and η_i are stable gain parameters.

Based on (25) and (26), the subsystem control law can be expressed as

$$\begin{aligned} u_{e1} &= g_1^{-1}\left[\ddot{x}_d + \frac{1}{2k_1}\mathcal{D}^{\alpha+2}\{e_x(t)\} + \frac{k_1}{2}\mathcal{D}^{2-\alpha}\{e_x(t)\} \right. \\ &\quad \left. - f_1 + \mu_1 sign(\dot{S}_1) + \eta_1 S_1\right] \\ u_{e2} &= g_2^{-1}\left[\ddot{\varphi}_d + \frac{1}{2k_2}\mathcal{D}^{\alpha+2}\{e_\varphi(t)\} + \frac{k_2}{2}\mathcal{D}^{2-\alpha}\{e_\varphi(t)\} \right. \\ &\quad \left. - f_2 + \mu_2 sign(\dot{S}_2) + \eta_2 S_2\right] \end{aligned} \tag{27}$$

Ideally, the controller has strong robustness when the stable gain shown in (27) is greater than the upper bound of unknown disturbances. However, in practical applications, we can only set the stable gain parameters to a very large value in order to cope with the unclear upper bound of unknown disturbances [35]. Because of the inevitable defects of the controller in the stabilization stage and the delay in the control process, the above processing method can lead to abnormal oscillation of the control system, which is very harmful to the spherical robot system. Faced with HSMC, the defects of the subsystems in the control process will eventually be superposed and coupled in the total control law of the system. If we process the defects in the second layer sliding surface, the difficulty of processing will increase, leading to the increase of control error of the spherical robot eventually. Therefore, according to the stable gain parameters μ_i and η_i of the subsystem stable control law $u_{ei-s}(t)$, we propose an adaptive estimation of its first derivative, as shown in (28).

$$\begin{aligned} \dot{\hat{\mu}}_i &= \rho_i S sign\left(\dot{S}_i\right) \\ \dot{\hat{\eta}}_i &= \kappa_i S S_i \end{aligned} \tag{28}$$

where $\dot{\hat{\mu}}_i$ and $\dot{\hat{\eta}}_i$ are the estimated values of the stable gain parameters $\dot{\mu}_i$ and $\dot{\eta}_i$, ρ_i and κ_i are the adaptive speed constants of the stable gain parameters, and both ρ_i and κ_i are positive numbers.

Therefore, the adaptive subsystem control laws of the F-AIHSMC are shown in (29), respectively.

$$\begin{aligned} u_{e1} &= g_1^{-1}\left[\ddot{x}_d + \frac{1}{2k_1}\mathcal{D}^{\alpha+2}\{e_x(t)\} + \frac{k_1}{2}\mathcal{D}^{2-\alpha}\{e_x(t)\} \right. \\ &\quad \left. - f_1 + \hat{\mu}_1 sign(\dot{S}_1) + \hat{\eta}_1 S_1\right] \\ u_{e2} &= g_2^{-1}\left[\ddot{\varphi}_d + \frac{1}{2k_2}\mathcal{D}^{\alpha+2}\{e_\varphi(t)\} + \frac{k_2}{2}\mathcal{D}^{2-\alpha}\{e_\varphi(t)\} \right. \\ &\quad \left. - f_2 + \hat{\mu}_2 sign(\dot{S}_2) + \hat{\eta}_2 S_2\right] \end{aligned} \tag{29}$$

D. CONSTRUCTION OF THE SECOND LAYER SLIDING SURFACE

The second layer sliding surface $S(t)$ is as follows [36].

$$S(t) = c_1 \cdot \dot{S}_1(t) + c_2 \cdot \dot{S}_2(t) \tag{30}$$

where $c_1 > 0$, $c_2 > 0$. Basing on the adaptive subsystem control laws shown in (29), we calculate one derivative of (30)

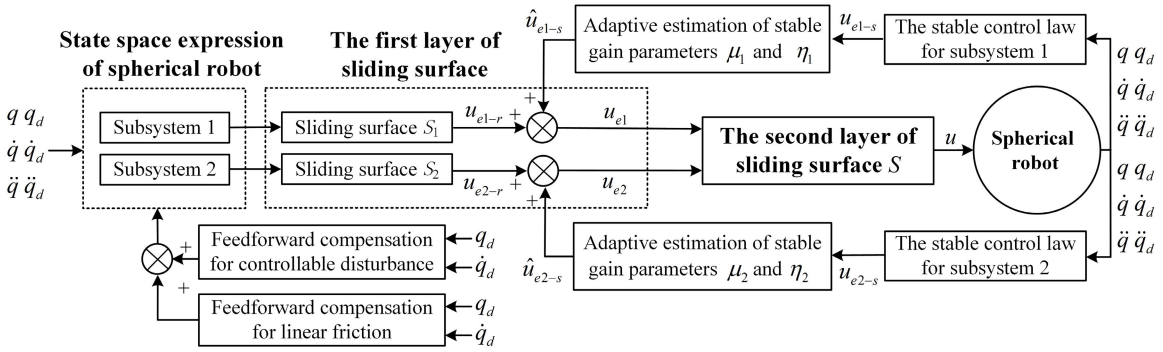

FIGURE 2. The structure of the F-AIHSMC.

with respect to time, and $\dot{S}(t)$ is

$$\begin{aligned}\dot{S}(t) = {} & c_1\mathcal{D}^{\alpha+2}\{e_x(t)\} + 2c_1k_1(\ddot{x}_d - f_1 - g_1u_{e1} - \xi_1) \\ & + c_2\mathcal{D}^{\alpha+2}\{e_\varphi(t)\} + 2c_2k_2(\ddot{\varphi}_d - f_2 - g_2u_{e2} - \xi_2) \\ & + c_1k_1^2\mathcal{D}^{2-\alpha}\{e_x(t)\} + c_2k_2^2\mathcal{D}^{2-\alpha}\{e_\varphi(t)\} \end{aligned} \tag{31}$$

In order to make the second sliding variable $S(t)$ converge to 0 rapidly, we use the exponential approach law, as shown in (32), to design the F-AIHSMC.

$$\dot{S}(t) = -\varepsilon_1 \cdot S - \varepsilon_2 \cdot sign(S) \tag{32}$$

where ε_1, ε_2 are constants greater than 0. According to (31) and (32), the approach control law $u_{sw}(t)$ can be obtained as follows.

$$\begin{aligned} u_{sw} = {} & -\frac{2c_2k_2g_2}{2c_1k_1g_1 + 2c_2k_2g_2}u_{e1} - \frac{2c_1k_1g_1}{2c_1k_1g_1 + 2c_2k_2g_2}u_{e2} \\ & + \frac{\varepsilon_1 \cdot S + \varepsilon_2 \cdot sign(S)}{2c_1k_1g_1 + 2c_2k_2g_2} \end{aligned} \tag{33}$$

By bringing (33) into (19), the control law of F-AIHSMC can be obtained, as shown in (34).

$$\begin{aligned} u(t) &= u_{e1}(t) + u_{e2}(t) + u_{sw}(t) \\ &= \frac{2c_1k_1g_1}{2c_1k_1g_1 + 2c_2k_2g_2}u_{e1} + \frac{2c_2k_2g_2}{2c_1k_1g_1 + 2c_2k_2g_2}u_{e2} \\ &\quad + \frac{\varepsilon_1 \cdot S + \varepsilon_2 \cdot sign(S)}{2c_1k_1g_1 + 2c_2k_2g_2} \end{aligned} \tag{34}$$

The structure of the F-AIHSMC is shown in Fig.2. According to the F-AIHSMC, we can obtain the following theorems:

Theorem 1: Assume that the desired motion trajectory of the linear motion of a spherical robot is a continuous and bounded function in the range of $[0 \quad +\infty)$. For a spherical robot system having the dynamic model shown in (9), if (29) is taken as the control law of the subsystems, and (34) is taken as the control law of the total system, then $\lim_{t\to\infty} ||(e_x \ e_\varphi)^T|| = 0$ can be realized.

Proof: Select Lyapunov function as follows:

$$V = \frac{1}{2}S^2 + \sum_{i=1}^{2}\left(\frac{1}{2\kappa_i}\hat{\eta}_i^2 + \frac{c_ik_i}{\rho_i}\hat{\mu}_i^2\right)$$

According to (28), we can compute the derivative of V as follows:

$$\begin{aligned} \dot{V} &= S\dot{S} + \frac{1}{\kappa_1}\hat{\eta}_1\dot{\hat{\eta}}_1 + \frac{1}{\kappa_2}\hat{\eta}_2\dot{\hat{\eta}}_2 + \frac{2c_1k_1}{\rho_1}\hat{\mu}_1\dot{\hat{\mu}}_1 + \frac{2c_2k_2}{\rho_2}\hat{\mu}_2\dot{\hat{\mu}}_2 \\ &= S\dot{S} + \hat{\eta}_1S\dot{S}_1 + \hat{\eta}_2S\dot{S}_2 + 2c_1k_1\hat{\mu}_1Ssign(\dot{S}_1) \\ &\quad + 2c_2k_2\hat{\mu}_2Ssign(\dot{S}_2) \\ &= S\Big[c_1\mathcal{D}^{\alpha+2}\{e_x(t)\} + 2c_1k_1(\ddot{x}_d - f_1 - g_1u_{e1} - \xi_1) \\ &\quad + c_2\mathcal{D}^{\alpha+2}\{e_\varphi(t)\} + 2c_2k_2(\ddot{\varphi}_d - f_2 - g_2u_{e2} - \xi_2) \\ &\quad + c_1k_1^2\mathcal{D}^{2-\alpha}\{e_x(t)\} + c_2k_2^2\mathcal{D}^{2-\alpha}\{e_\varphi(t)\}\Big] + \hat{\eta}_1S\dot{S}_1 \\ &\quad + \hat{\eta}_2S\dot{S}_2 + 2c_1k_1\hat{\mu}_1Ssign(\dot{S}_1) + 2c_2k_2\hat{\mu}_2Ssign(\dot{S}_2) \\ &= S\Big[c_1\mathcal{D}^{\alpha+2}\{e_x(t)\} + 2c_1k_1(\ddot{x}_d - f_1 - \xi_1) \\ &\quad + c_1k_1^2\mathcal{D}^{2-\alpha}\{e_x(t)\} + c_2\mathcal{D}^{\alpha+2}\{e_\varphi(t)\} \\ &\quad + 2c_2k_2(\ddot{\varphi}_d - f_2 - \xi_2) + c_2k_2^2\mathcal{D}^{2-\alpha}\{e_\varphi(t)\} \\ &\quad - (2k_1c_1g_1 + 2k_2c_2g_2)u\Big] + \hat{\eta}_1S\dot{S}_1 + \hat{\eta}_2S\dot{S}_2 \\ &\quad + 2c_1k_1\hat{\mu}_1Ssign(\dot{S}_1) + 2c_2k_2\hat{\mu}_2Ssign(\dot{S}_2) \end{aligned} \tag{35}$$

By bringing (34) into (35), we can obtain one derivative of V with respect to time, as shown in (36).

$$\begin{aligned} \dot{V} &= S\left[-\varepsilon_1 \cdot S - \varepsilon_2 sign(S) - \hat{\eta}_1S_1 - \hat{\eta}_2S_2\right. \\ &\quad \left. - \ 2c_1k_1\hat{\mu}_1sign(\dot{S}_1) - 2c_2k_2\hat{\mu}_2sign(\dot{S}_2)\right] + \hat{\eta}_1S\dot{S}_1 \\ &\quad + \hat{\eta}_2S\dot{S}_2 + 2c_1k_1\hat{\mu}_1Ssign(\dot{S}_1) + 2c_2k_2\hat{\mu}_2Ssign(\dot{S}_2) \\ &= -\varepsilon_1 \cdot S^2 - \varepsilon_2|S| \end{aligned} \tag{36}$$

According to (36), $\dot{V} \leq 0$, and $\dot{V} = 0$ if and only if $S = 0$. According to the Lasalle's invariance principle, the linear motion of the spherical robot is asymptotically stable under the control law (34).

The subsystems also need to be asymptotically stable.

Select Lyapunov function as follows:

$$V = \frac{1}{2}S_i^2 + \frac{1}{2}\dot{S}_i^2$$

According to (23) and (29), we can compute the derivative of V as follows:

$$\begin{aligned} \dot{V} &= S_i\dot{S}_i + \dot{S}_i\ddot{S}_i = S_i\dot{S}_i + \dot{S}_i\{-2k_i\hat{\mu}_isign(\dot{S}_i) - 2k_i\hat{\eta}_iS_i - \xi_i\} \\ &= S_i\dot{S}_i - 2k_i\hat{\eta}_i\dot{S}_iS_i - 2k_i\hat{\mu}_i\dot{S}_isign(\dot{S}_i) - \dot{S}_i\xi_i \\ &\leq S_i\dot{S}_i - 2k_i\hat{\eta}_i\dot{S}_iS_i - 2k_i\hat{\mu}_i|\dot{S}_i| + |\dot{S}_i\xi_{i-\max}| \\ &\leq |\dot{S}_i|\{(|\xi_{i-\max}| - 2k_i\hat{\mu}_i) + |S_i|(1 - 2k_i\hat{\eta}_i)\} \end{aligned}$$

When the parameter k_i of the first layer sliding surface S_i satisfies $k_i\hat{\eta}_i > 1/2$ and $k_i\hat{\mu}_i > |\xi_{i-\max}|/2$, the subsystem i is asymptotically stable. The proof of Theorem 1 is done.

Theorem 1 proves that the system is asymptotically stable. In the F-AIHSMC, the first layer sliding surfaces S_i and the second layer sliding surface S also need to be asymptotically stable.

Theorem 2: Assume that the desired motion trajectory of the linear motion of a spherical robot is a continuous and bounded function in the range of $[0 \quad +\infty)$. For a spherical robot system having the dynamic model shown in (9), under the control law (34), the first layer sliding surfaces S_i and the second layer sliding surface S are asymptotically stable.

Proof: By integrating (36), we can obtain

$$\begin{aligned}\int_0^t \dot{V}d\omega &= \int_0^t (-\varepsilon_1 \cdot S^2 - \varepsilon_2|S|)d\omega \\ V(t) - V(0) &= \int_0^t (-\varepsilon_1 \cdot S^2 - \varepsilon_2|S|)d\omega \\ V(0) - V(t) &= \int_0^t (\varepsilon_1 \cdot S^2 + \varepsilon_2|S|)d\omega \end{aligned} \tag{37}$$

Because $\dot{V} \leq 0$, therefore, $V(t) < V(0) < \infty$, according to (37):

$$\begin{aligned} V(0) &= \int_0^t (\varepsilon_1 \cdot S^2 + \varepsilon_2|S|)d\omega + V(t) \\ &\leq \int_0^t (\varepsilon_1 \cdot S^2 + \varepsilon_2|S|)d\omega < \infty \end{aligned} \tag{38}$$

Since ε_1 and ε_2 are positive real numbers, therefore $S < \infty$ can be obtained. By bringing it into $\dot{V} = S\dot{S} = -\varepsilon_1 \cdot S^2 - \varepsilon_2|S| < \infty$, we can obtain $\dot{S} < \infty$. According to Barbalat lemma [37], we can conclude that:

$$\lim_{t\to\infty}(\varepsilon_1 \cdot S^2 + \varepsilon_2|S|) = 0 \quad \lim_{t\to\infty} S = 0$$

According to (38), whether the sliding surface S is stable is independent of ε_1 and ε_2. Therefore, we assume two different sliding surfaces S_A and S_B, as shown in (39), and the parameters c_{A1}, c_{A1} and c_2 are all positive real numbers.

$$\begin{aligned} S_A(t) &= c_{A1} \cdot \dot{S}_1(t) + c_2 \cdot \dot{S}_2(t) \\ S_B(t) &= c_{B1} \cdot \dot{S}_1(t) + c_2 \cdot \dot{S}_2(t) \end{aligned} \tag{39}$$

Let $S_A(t) > S_B(t)$, we can get the result shown in (40).

$$\begin{aligned} &\int_0^t \left(S_A^2 - S_B^2\right) d\omega \\ &= \int_0^t [(c_{A1} \cdot \dot{S}_1 + c_2 \cdot \dot{S}_2)^2 - (c_{B1} \cdot \dot{S}_1 + c_2 \cdot \dot{S}_2)^2]d\omega \\ &= \int_0^t [c_{A1}^2\dot{S}_1^2 + 2c_{A1}c_2\dot{S}_1\dot{S}_2 - c_{B1}^2\dot{S}_1^2 - 2c_{B1}c_2\dot{S}_1\dot{S}_2]d\omega \\ &= \int_0^t [(c_{A1}^2 - c_{B1}^2)\dot{S}_1^2 + 2c_2(c_{A1} - c_{B1})\dot{S}_1\dot{S}_2]d\omega \\ &= \int_0^t [2c_{A1}^2\dot{S}_1^2 - c_{A1}^2\dot{S}_1^2 - c_{B1}^2\dot{S}_1^2 + 2c_{A1}c_2\dot{S}_1\dot{S}_2 \\ &\quad - 2c_{B1}c_2\dot{S}_1\dot{S}_2 + 2c_{A1}c_{B1}\dot{S}_1^2 - 2c_{A1}c_{B1}\dot{S}_1^2]d\omega \\ &= \int_0^t [(-c_{A1}^2 + 2c_{A1}c_{B1} - c_{B1}^2)\dot{S}_1^2 \\ &\quad + 2(c_{A1}^2\dot{S}_1^2 - c_{A1}c_{B1}\dot{S}_1^2 + c_{A1}c_2\dot{S}_1\dot{S}_2 - c_{B1}c_2\dot{S}_1\dot{S}_2)]d\omega \\ &= \int_0^t [(-c_{A1}^2 + 2c_{A1}c_{B1} - c_{B1}^2)\dot{S}_1^2 \\ &\quad + 2(c_{A1} - c_{B1})(c_{A1} \cdot \dot{S}_1 + c_2 \cdot \dot{S}_2)\dot{S}_1]d\omega \\ &= \int_0^t [-(c_{A1} - c_{B1})^2\dot{S}_1^2 + 2(c_{A1} - c_{B1})S_A\dot{S}_1]d\omega \end{aligned} \tag{40}$$

According to (40), $\dot{S}_1 < \infty$ can be obtained. Since $\dot{S} < 0$, according to the Lemma 4 in [37], we can conclude that:

$$\lim_{t\to\infty} S_1 = 0$$

Using the same proof method, we can conclude that:

$$\lim_{t\to\infty} S_2 = 0$$

Therefore, the first layer sliding surfaces S_i and the second layer sliding surface S are asymptotically stable. The proof of Theorem 2 is done.

According to the control law proposed in (34), if the stable gain parameters increase, the *signum* function (*sign*) can cause the increase of system chattering. Therefore, in order to avoid the above situation, we modify the control law of F-AIHSMC to:

$$\begin{aligned} u(t) &= u_{e1}(t) + u_{e2}(t) + u_{sw}(t) \\ &= \frac{2c_1k_1g_1}{2c_1k_1g_1 + 2c_2k_2g_2}u_{e1} + \frac{2c_2k_2g_2}{2c_1k_1g_1 + 2c_2k_2g_2}u_{e2} \\ &\quad + \frac{\varepsilon_1 \cdot S + \varepsilon_2 \tanh(S)}{2c_1k_1g_1 + 2c_2k_2g_2} \end{aligned} \tag{41}$$

The adaptive subsystem control laws of the F-AIHSMC are modified as follows:

$$\begin{aligned} u_{e1}(t) &= g_1^{-1}[\ddot{x}_d + \frac{1}{2k_1}\mathcal{D}^{\alpha+2}\{e_x(t)\} \\ &\quad + \frac{k_1}{2}\mathcal{D}^{2-\alpha}\{e_x(t)\} - f_1 + \hat{\mu}_1 sat(\dot{S}_1) + \hat{\eta}_1 S_1] \\ u_{e2}(t) &= g_2^{-1}[\ddot{\varphi}_d + \frac{1}{2k_2}\mathcal{D}^{\alpha+2}\{e_\varphi(t)\} \\ &\quad + \frac{k_2}{2}\mathcal{D}^{2-\alpha}\{e_\varphi(t)\} - f_2 + \hat{\mu}_2 sat(\dot{S}_2) + \hat{\eta}_2 S_2] \end{aligned} \tag{42}$$

where

$$tanh(x) = (e^x - e^{-x})/(e^x + e^{-x})$$

$$sat(\dot{S}) = \begin{cases} sign(\dot{S}), & |\dot{S}| > \varpi > 0 \\ \dot{S}/\varpi, & |\dot{S}| \leq \varpi \end{cases}$$

$x \in R$, ϖ is a positive constant.

IV. EXPERIMENTAL STUDIES

In order to verify the effectiveness of the F-AIHSMC, we used the BYQ-GS spherical robot to carry out the experiment of high-speed linear motion. For comparison, the same high-speed linear motion experiments using the traditional HSMC and the AHSMC proposed in [22] were also performed.

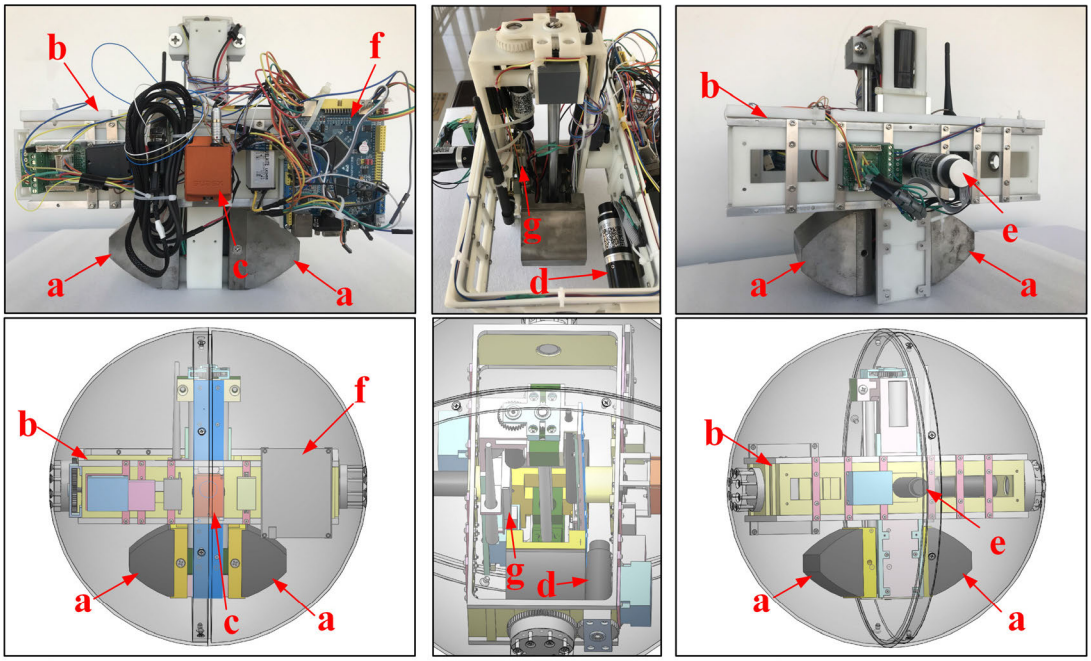

FIGURE 3. The 3D model and physical prototype of the BYQ-GS spherical robot. (a) Weight pendulum integrated into power system. (b) Lightweight main frame. (c) Xsens MTi-300 inertial attitude measurement system. (d) DC brushless motor (absolute encoder) in long axis direction. (e) DC brushless motor (absolute encoder) in short axis direction. (f) Embedded main control board. (g) Trimble BD982 high-precision RTK positioning board.

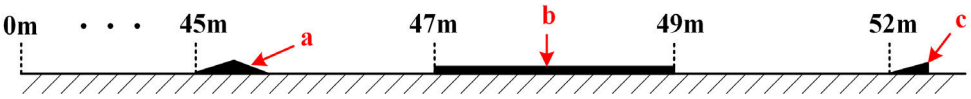

FIGURE 4. Schematic diagram of the experimental field. (a) Bi-directional short ramp. (b) Thick sponge track. (c) Uni-directional short ramp.

A. EXPERIMENTAL PLATFORM

The 3D model and physical prototype of the BYQ-GS spherical robot are shown in Fig.3, and its performance parameters are shown in Table 1. Compared with the traditional spherical robot driven by the eccentric torque driving mechanism based on weight pendulum, the BYQ-GS spherical robot can satisfy the requirements of high-speed motion tasks. According to the lightweight design principle, we used the combination of the glass fiber reinforced polymer spherical shell and the photosensitive resin frame based on 3D printing technology. The internal structure was optimized by topology optimization design, and the weight pendulum and the power system were functionally integrated. Under the premise of a large reduction of the overall mass, the high proportion of the weight pendulum mass relative to the overall mass can be ensured, so that the high-speed and flexible movement of the BYQ-GS spherical robot can be realized. By combining DC brushless motor with absolute encoder, Xsens MTi-300 inertial attitude measurement system and Trimble BD982 high-precision RTK positioning board, we can make the BYQ-GS spherical robot have the ability to control and measure the motion process.

TABLE 1. Performance parameters of BYQ-GS spherical robot.

Parameter type	Parameter value
Maximum speed	8m/s
Maximum acceleration	3m/s^2
External diameter	400mm
Overall mass	10kg
Weight pendulum mass	6.9kg
Pendulum arm length	124mm
Battery life	1.5h
Operating error	≤3cm

The schematic diagram of the experimental field is shown in Fig.4. A 15° bi-directional short ramp was set at the 45m displacement, a 2m long and 30mm thick sponge track was set at the 47m displacement, and a 15° uni-directional short ramp was set at the 52m displacement. The purpose of the above setting is to simulate complicated disturbances caused by various road conditions in actual working conditions.

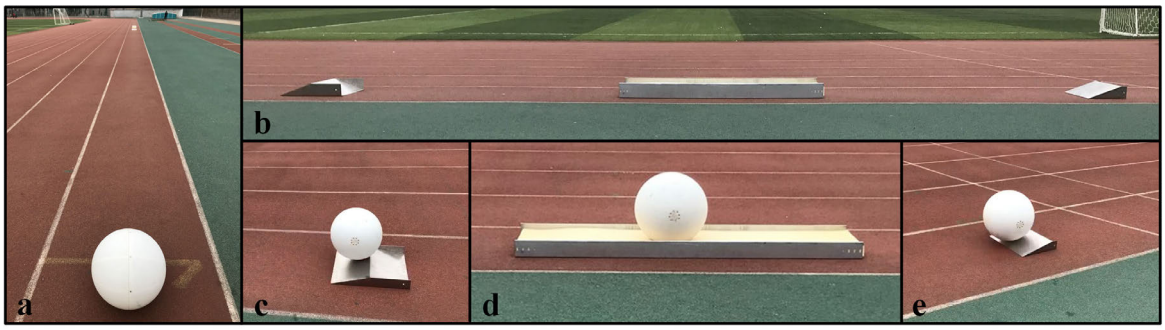

FIGURE 5. The experimental scene. (a) Initial state. (b) Disturbance simulation area. (c) BYQ-GS passing through the bi-directional short ramp during operation. (d) BYQ-GS passing through the thick sponge track during operation. (e) BYQ-GS passing through the uni-directional short ramp during operation.

TABLE 2. Motion control effect of three controllers in experiment 1.

Stage	Indicator		F-AIHSMC	AHSMC	HSMC
Stage 1	t_r (s)		7.21	8.07	9.57
	$e_{x\text{-max}}$ (m)		3.174	3.455	3.891
	$e_{x\text{-}RMSE}$		1.535	1.739	2.267
	$e_{\varphi\text{-max}}$ (m)		0.229	0.244	0.257
	$e_{\varphi\text{-}RMSE}$		0.089	0.117	0.127
Stage 2	t_r (s)	D1	0.26	0.46	2.02
		D2	0.93	1.15	
		D3	0.42	0.56	0.71
	$e_{x\text{-max}}$ (m)		0.061	0.082	0.113
	$e_{x\text{-}RMSE}$		0.013	0.018	0.037
	$e_{\varphi\text{-max}}$ (m)		$1.396*10^{-2}$	$1.668*10^{-2}$	$1.992*10^{-2}$
	$e_{\varphi\text{-}RMSE}$		$3.124*10^{-3}$	$4.033*10^{-3}$	$4.564*10^{-3}$

Stage 1 is the initial control stage. Stage 2 is the disturbance control stage. D1 is the bi-directional short ramp in the experimental field. D2 is the thick sponge track in the experimental field. D3 is the uni-directional short ramp in the experimental field.

B. DETERMINATION OF THE OPTIMAL PARAMETERS OF F-AIHSMC

In order to determine the optimal parameters of the F-AIHSMC, we first ignored the fractional calculus, that is, the α in (21) was 1, and used the Global Optimization Toolbox in MATLAB to determine the optimal values of control parameters $(k_1, k_2, c_1, c_2, \varepsilon_1, \varepsilon_2)$ and adaptive law parameters $(\rho_1, \rho_2, \kappa_1, \kappa_2)$ through the pattern search method. The optimal parameters for the convergence speed and precise control performance of the F-AIHSMC were obtained, as shown below.

$$(k_1, k_2, c_1, c_2, \varepsilon_1, \varepsilon_2) = (0.697, 2.187, 5.896, 3.434, 10.103, 0.117)$$
$$(\rho_1, \rho_2, \kappa_1, \kappa_2) = (17.3, 21.8, 12.2, 14.9)$$

According to the above optimal parameters, we used the FOMCON (fractional-order modeling and control toolbox) in MATLAB and adjusted the α of fractional calculus by trial and error method. The optimal value of α is 0.65.

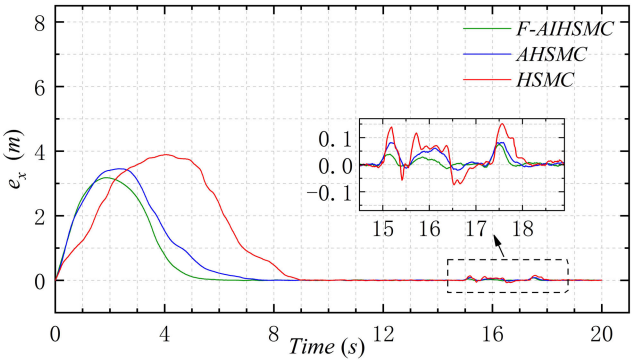

FIGURE 6. Comparison of relevant data variations of sub-experiments of experiment 1.

C. EXPERIMENTAL PROCESS AND RESULTS

We set up three sets of experiments according to different expected states. In each set of experiment, three different control methods were applied to the high-speed linear motion of the BYQ-GS spherical robot as three sub-experiments of each set of experiment. In order to ensure the reliability of the data and compare the results intuitively, we did 10 replicates during the sub-experiment and took the average, and then preprocessed the data using the Savizkg-Golag smoothing algorithm (30 points and 2 times) to get the final data. Based on the obtained data, we compared the control effects of F-AIHSMC proposed in this study, AHSMC proposed in [22], and classical HSMC. In this study, the control process of first-time converging of BYQ-GS spherical robot to the desired state was defined as the initial control stage, and the control process after being disturbed was defined as the disturbance control stage. We used three indicators, i.e. convergence time t_r, maximum absolute value of motion trajectory error $e_{\max}$, root mean square error (RMSE) value of motion trajectory error e_{RMSE}, to show the control effects of the three controllers clearly. The experimental scene is shown in Fig.5.

TABLE 3. Motion control effect of three controllers in experiment 2.

Stage	Indicator		F-AIHSMC	AHSMC	HSMC
Stage 1	t_r (s)		7.77	9.13	11.97
	$e_{x\text{-max}}$ (m)		3.528	3.954	4.729
	$e_{x\text{-RMSE}}$		1.673	1.938	2.549
	$e_{\varphi\text{-max}}$ (m)		0.242	0.261	0.274
	$e_{\varphi\text{-RMSE}}$		0.100	0.146	0.149
Stage 2	t_r (s)	D1	0.46	2.01	3.61
		D2	0.96		
		D3	0.65	0.83	
	$e_{x\text{-max}}$ (m)		0.090	0.125	0.186
	$e_{x\text{-RMSE}}$		0.017	0.025	0.059
	$e_{\varphi\text{-max}}$ (m)		$1.594*10^{-2}$	$2.048*10^{-2}$	$2.921*10^{-2}$
	$e_{\varphi\text{-RMSE}}$		$4.636*10^{-3}$	$6.408*10^{-3}$	$7.602*10^{-3}$

Stage 1 is the initial control stage. Stage 2 is the disturbance control stage. D1 is the bi-directional short ramp in the experimental field. D2 is the thick sponge track in the experimental field. D3 is the uni-directional short ramp in the experimental field.

TABLE 4. Motion control effect of three controllers in experiment 3.

Stage	Indicator		F-AIHSMC	AHSMC	HSMC
Stage 1	t_r (s)		8.82	10.73	------
	$e_{x\text{-max}}$ (m)		4.633	5.380	6.417
	$e_{x\text{-RMSE}}$		2.577	3.170	4.171
	$e_{\varphi\text{-max}}$ (m)		0.311	0.355	0.358
	$e_{\varphi\text{-RMSE}}$		0.177	0.279	0.291
Stage 2	t_r (s)	D1	0.36	2.85	3.65
		D2	1.04		
		D3	0.52		
	$e_{x\text{-max}}$ (m)		0.115	0.167	0.349
	$e_{x\text{-RMSE}}$		0.022	0.035	0.097
	$e_{\varphi\text{-max}}$ (m)		$1.932*10^{-2}$	$2.586*10^{-2}$	$4.427*10^{-2}$
	$e_{\varphi\text{-RMSE}}$		$5.402*10^{-3}$	$8.994*10^{-3}$	$1.361*10^{-2}$

Stage 1 is the initial control stage. Stage 2 is the disturbance control stage. D1 is the bi-directional short ramp in the experimental field. D2 is the thick sponge track in the experimental field. D3 is the uni-directional short ramp in the experimental field.

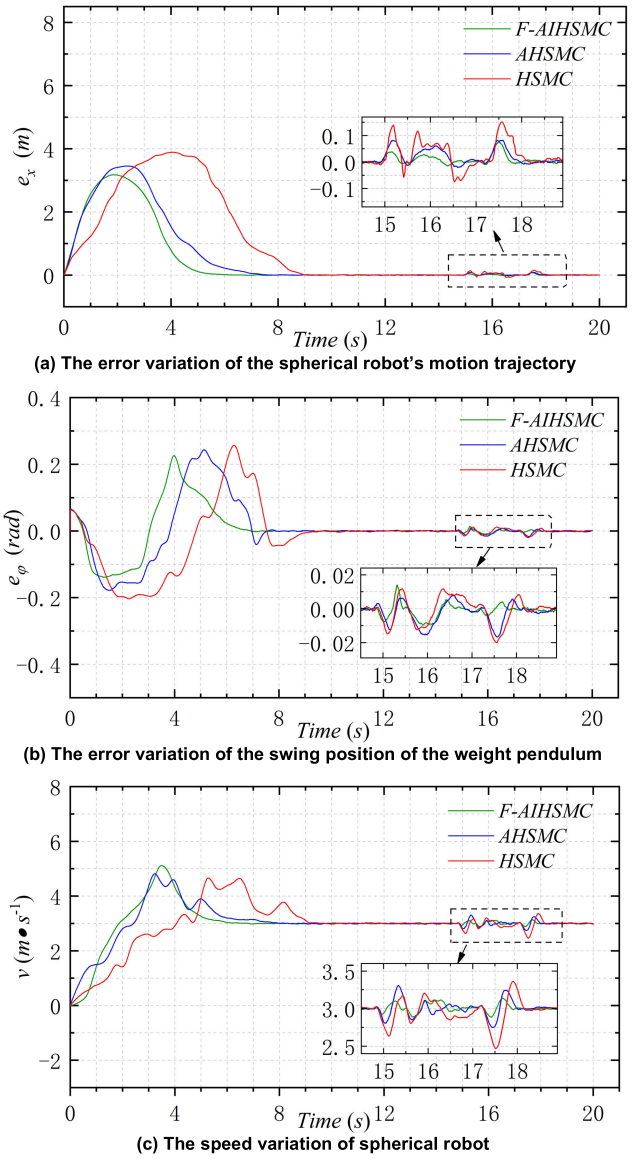

FIGURE 7. Comparison of relevant data variations of sub-experiments of experiment 2.

1) EXPERIMENT 1

The initial state of spherical robot system is $(x_0, \varphi_0) = (0, 0)$, and the expected state of linear motion is $(x_d, \varphi_d) = (3t, \tau_r / m_3 g L)$. The error of the motion trajectory $e_x(t) = x_d(t) - x(t)$, the error of the swing position of the weight pendulum $e_\varphi(t) = \varphi_d(t) - \varphi(t)$, and the speed variation of the spherical robot are shown in Fig.6.

The initial control stage of experiment 1 is defined as 0-10s, and the disturbance control stage is defined as 10-20s. The linear motion control effects of the three controllers are shown in Table 2.

2) EXPERIMENT 2

The initial state of spherical robot system is $(x_0, \varphi_0) = (0, 0)$, and the expected state of linear motion is $(x_d, \varphi_d) = (3.5t, \tau_r / m_3 g L)$. The error of the motion trajectory $e_x(t) = x_d(t) - x(t)$, the error of the swing position of the weight pendulum $e_\varphi(t) = \varphi_d(t) - \varphi(t)$, and the speed variation of the spherical robot are shown in Fig.7.

The initial control stage of experiment 2 is defined as 0-12s, and the disturbance control stage is defined as 12-20s. The linear motion control effects of the three controllers are shown in Table 3.

3) EXPERIMENT 3

The initial state of spherical robot system is $(x_0, \varphi_0) = (0, 0)$, and the expected state of linear motion is $(x_d, \varphi_d) = (4t, \tau_r / m_3 g L)$. The error of the motion trajectory $e_x(t) = x_d(t) - x(t)$,the error of the swing position of

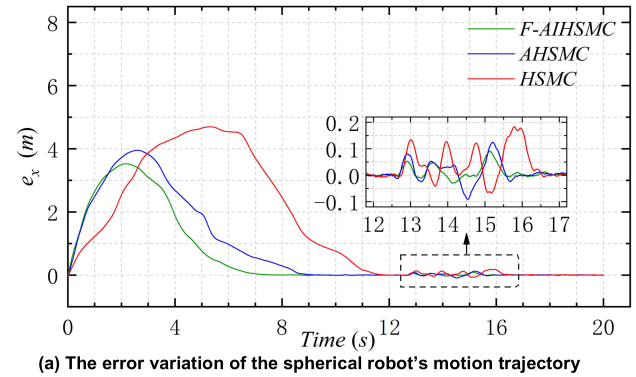

(a) The error variation of the spherical robot's motion trajectory

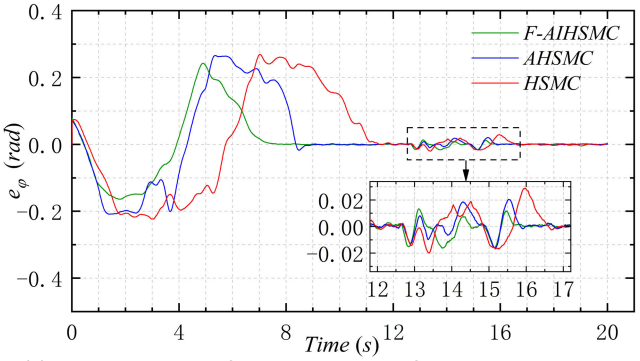

(b) The error variation of the swing position of the weight pendulum

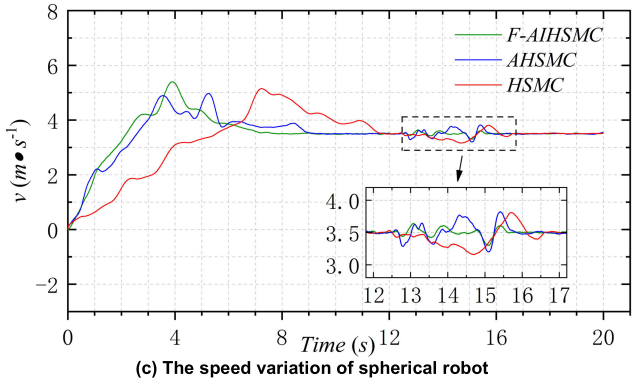

(c) The speed variation of spherical robot

FIGURE 8. Comparison of relevant data variations of sub-experiments of experiment 3.

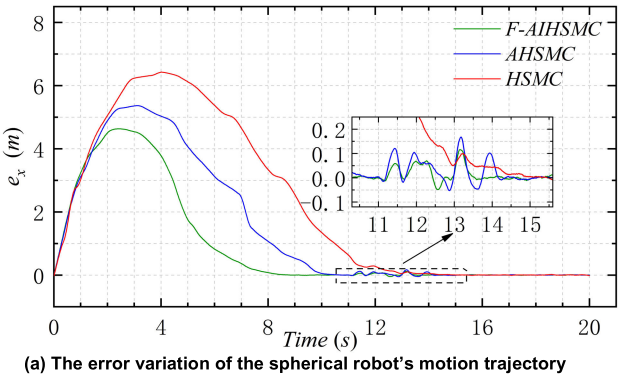

(a) The error variation of the spherical robot's motion trajectory

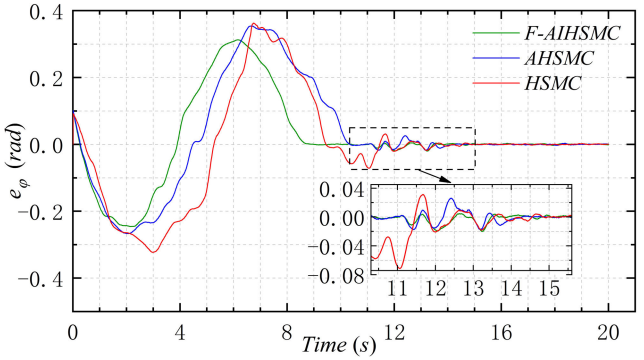

(b) The error variation of the swing position of the weight pendulum

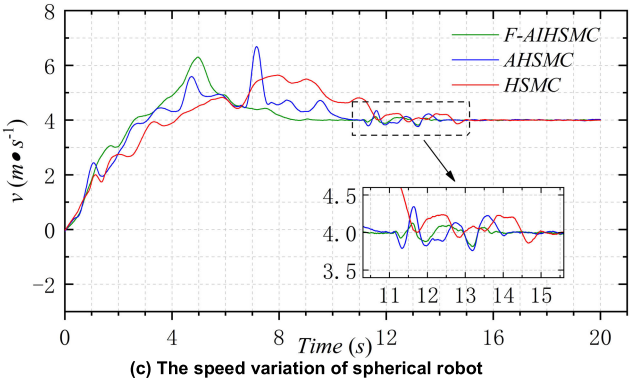

(c) The speed variation of spherical robot

FIGURE 9. Comparison of the control signal changes of the three control methods.

the weight pendulum $e_\varphi(t) = \varphi_d(t) - \varphi(t)$, and the speed variation of the spherical robot are shown in Fig.8.

When HSMC was used for linear motion control of the spherical robot in experiment 3, the BYQ-GS spherical robot failed to achieve first-time convergence to the expected state before encountering disturbance 1. Therefore, the expected time to reach disturbance 1 was the dividing point of the two stages, that is, the initial control stage of experiment 3 is defined as 0-11.25s, and the disturbance control stage is 11.25-20s. The linear motion control effects of the three controllers are shown in Table 4.

4) ANALYSIS OF RESULTS

According to the data above, we compared the control effects of F-AIHSMC and AHSMC, F-AIHSMC and HSMC in the two control stages, respectively. The comparison results are shown in Table 5.

According to the three sets of data and comparison results (Table 5), the three indicators of F-AIHSMC t_r, $e_{\max}$ and e_{RMSE} are all the best. In the initial control stage of the three sets of experiments, both F-AIHSMC and AHSMC can converge. However, when the expected speed is 4m/s, HSMC fails to achieve convergence. In the disturbance control stage of the three sets of experiments, when the BYQ-GS spherical robot faces disturbances at three fixed positions, F-AIHSMC can achieve rapid convergence. In the second and third sets of experiments, AHSMC cannot achieve simultaneous convergence of the three disturbances when the expected speed reaches to higher than 3.5m/s. HSMC cannot achieve simultaneous convergence of the three disturbances in all three sets of

TABLE 5. Comparison results of F-AIHSMC and the other two control methods.

Stage	Controller	Experiment	Indicator						
			t_r			$e_{x\text{-max}}$	$e_{x\text{-}RMSE}$	$e_{\varphi\text{-max}}$	$e_{\varphi\text{-}RMSE}$
Stage 1	AHSMC	1	↓10.66%			↓8.13%	↓11.73%	↓6.15%	↓23.93%
		2	↓14.89%			↓10.77%	↓13.67%	↓7.28%	↓31.51%
		3	↓17.80%			↓13.88%	↓18.71%	↓12.39%	↓36.66%
	HSMC	1	↓24.67%			↓18.43%	↓32.29%	↓10.89%	↓29.92%
		2	↓35.08%			↓25.40%	↓34.36%	↓11.68%	↓32.76%
		3	——			↓27.80%	↓38.22%	↓13.13%	↓39.18%
Stage 2	AHSMC	1	D1: ↓43.47%	D2: ↓19.13%	D3: ↓25.00%	↓25.61%	↓27.78%	↓16.31%	↓22.53%
		2	D1: ——	D2: ——	D3: ↓28.23%	↓27.73%	↓33.25%	↓22.39%	↓27.65%
		3	D1: ——	D2: ——	D3: ——	↓31.13%	↓37.14%	↓25.29%	↓39.94%
	HSMC	1	D1: ——	D2: ——	D3: ↓40.00%	↓46.02%	↓64.86%	↓36.13%	↓31.55%
		2	D1: ——	D2: ——	D3: ——	↓51.62%	↓71.13%	↓45.56%	↓39.16%
		3	D1: ——	D2: ——	D3: ——	↓67.04%	↓77.32%	↓56.14%	↓60.32%

Stage 1 is the initial control stage. Stage 2 is the disturbance control stage. D1 is the bi-directional short ramp in the experimental field. D2 is the thick sponge track in the experimental field. D3 is the uni-directional short ramp in the experimental field.

experiments. By comparing the t_r of the three sets of experiments, we can conclude that, compared with AHSMC and HSMC, F-AIHSMC has obvious advantages in increasing in the response speed and the convergence speed of the system. By combining the comparison of the $e_{\boldsymbol{x}-\max}$ and $e_{\varphi-\max}$ of the three sets of experiments with AHSMC and HSMC, F-AIHSMC has obvious advantage in reducing the system overshoot. By comparing the e_{x-RMSE} and $e_{\varphi-RMSE}$ of the three sets of experiments, and combining it with the change trend of the speed of spherical robot based on different control methods in the three sets of experiments, we can conclude that, compared with AHSMC and HSMC, F-AIHSMC has obvious advantage in enhancing the stability of the system. By comparing the convergence of the disturbance control stages of the three sets of experiments, we can conclude that compared with AHSMC and HSMC, F-AIHSMC can make the system more robust when facing unknown disturbances. Therefore, compared with AHSMC and HSMC, F-AIHSMC has the best control effect. With the increase of expected speed from 3m/s to 4m/s, the control advantage of F-AIHSMC becomes more and more obvious.

We extracted the data of the control signal τ without preprocessing in the three sets of experiments, and compared the control singal τ based on the three control methods, as shown in Fig.9.

Fig.9 shows that, when the speeds of high-speed motion are identical, the chattering of the controller can be better suppressed in F-AIHSMC compared with AHSMC and HSMC. With the increase of motion speed, although the effect of chattering suppression of F-AIHSMC is weakened, it still has obvious advantages over AHSMC and HSMC. From Fig.9, we can conclude that, by integrating integral sliding mode control and fractional calculus, and using $\tanh(S)$ and $sat(\dot{S})$ instead of the *signum* function $sign(S)$ and $sign(\dot{S})$, F-AIHSMC has a significant suppression effect on the chattering in high-speed linear motion control of spherical robot, which further reflects the strong stability of F-AIHSMC.

V. CONCLUSION

In this study, we focused on the problem of high-speed linear motion of the spherical robot. We carried out the study of linear motion adaptive control method for the spherical robot under high-speed motion through the combination of theory and experiment. We proposed F-AIHSMC by establishing the standard dynamic model for high-speed linear motion, and integrating the feedforward control method, integral term, fractional calculus and adaptive control method into HSMC basing on the standard dynamic model; Then, taking the BYQ-GS spherical robot as the experimental platform, we used F-AIHSMC to carry out the linear motion control experiments of the spherical robot. The results show that, when the spherical robot is in the high-speed linear motion process, compared with AHSMC with adaptive function and traditional HSMC, F-AIHSMC achieves high system response speed and convergence speed, and has stronger stability and robustness.

The spherical robot achieves high-speed and accurate linear motion through the study of F-AIHSMC. This study lays a solid foundation for the study of high-speed and precise omnidirectional motion control for the spherical robot. Moreover, it has an important guiding significance and promoting effect on application and popularization of the spherical robot.

REFERENCES

[1] Q. Zhan, "Research progress and development trend of spherical mobile robots," *J. Mech. Eng.*, vol. 55, no. 9, pp. 1–17, 2019.

[2] Y. S. Li, H. X. Sun, M. Chu, Y. H. Zhang, Q. X. Jia, and X. J. Lan, "Structure design and force analysis for a novel spherical robot," in *Proc. ICCAE*, Bangkok, Thailand, 2016, pp. 175–180.

[3] B. Alexey, K. Alexander, K. Yury, and K. Anton, "Stabilization of the motion of a spherical robot using feedbacks," *Appl. Math. Model.*, vol. 69, pp. 583–592, May 2019.

[4] H. Ghariblu, "A new mobile ball robot-dynamic modeling and simulation," *Appl. Math. Model.*, vol. 39, nos. 10–11, pp. 3103–3115, Jun. 2015.

[5] V. Muralidharan and A. D. Mahindrakar, "Geometric controllability and stabilization of spherical robot dynamics," *IEEE Trans. Autom. Control*, vol. 60, no. 10, pp. 2762–2767, Oct. 2015.
[6] E.-J. Jung, J. Hoon Lee, B.-J. Yi, I. Hong Suh, S. Yuta, and S. T. Noh, "Marathoner tracking algorithms for a high speed mobile robot," in *Proc. IEEE/RSJ Int. Conf. Intell. Robots Syst.*, San Francisco, CA. USA, Sep. 2011, pp. 3595–3600.
[7] Q. Hu, G. Ma, and L. Xie, "Robust and adaptive variable structure output feedback control of uncertain systems with input nonlinearity," *Automatica*, vol. 44, no. 2, pp. 552–559, Feb. 2008.
[8] Y. Ming, W. Sun, and P. Hu, "Sliding mode robust control for two-wheeled mobile robot with lower center of gravity," *Int. J. Innov. Comput. I.*, vol. 7, no. 2, pp. 637–646, Feb. 2011.
[9] M. Yue, W. Sun, and P. Hu, "Path following of a class of non-holonomic mobile robot with underactuated vehicle body," *IET Control Theory Appl.*, vol. 4, no. 10, pp. 1898–1904, Oct. 2010.
[10] Z. Ma and P. Huang, "Discrete-time sliding mode control for deployment of tethered space robot with only length and angle measurement," *IEEE Trans. Aerosp. Electron. Syst.*, vol. 56, no. 1, pp. 585–596, Feb. 2020.
[11] V.-A. Le, H.-X. Le, L. Nguyen, and M.-X. Phan, "An efficient adaptive hierarchical sliding mode control strategy using neural networks for 3D overhead cranes," *Int. J. Autom. Comput.*, vol. 16, no. 5, pp. 614–627, Oct. 2019.
[12] J. Liang, K. Y. Qin, and L. Chen, "Intelligent hierarchical sliding-mode control for flexible-joint space manipulator," *Chin. Q. Mech.*, vol. 40, no. 3, pp. 529–542, 2019.
[13] N. Xu, Y. Chen, A. Xue, G. Zong, and X. Zhao, "Event-trigger-based adap-tive fuzzy hierarchical sliding mode control of uncertain under-actuated switched nonlinear systems," *ISA Trans.*, to be published, doi: 10.1016/j.isatra.2019.11.011.
[14] H.-M. Wu and M. Karkoub, "Hierarchical fuzzy sliding-mode adaptive control for the trajectory tracking of differential-driven mobile robots," *Int. J. Fuzzy Syst.*, vol. 21, no. 1, pp. 33–49, Feb. 2019.
[15] Z. Ma and G. Sun, "Adaptive hierarchical sliding mode control with input saturation for attitude regulation of multi-satellite tethered system," *J. Astron. Sci.*, vol. 64, no. 2, pp. 207–230, Jun. 2017.
[16] V. T. Nguyen, K. D. Ha Thi, V. A. Le, T. D. Pham, H. T. Vo, and Q. T. Pham, "Modeling and integral hierarchical sliding-mode control for 2D ship-mounted crane," in *Proc. 1st Int. Symp. Instrum., Control, Artif. Intell., Robot. (ICA-SYMP)*, Bangkok, Thailand, Jan. 2019, pp. 82–85.
[17] D. Liu, H. Sun, and Q. Jia, "A family of spherical mobile robot: Driving ahead motion control by feedback linearization," in *Proc. 2nd Int. Symp. Syst. Control Aerosp. Astronaut.*, Shenzhen, China, Dec. 2008, pp. 700–705.
[18] B. Zhao, "Linear motion control of Two-pendulums-driven spherical robot," *J. Mech. Eng.*, vol. 47, no. 11, pp. 1–6, 2011.
[19] T. W. U. Madhushani, D. H. S. Maithripala, and J. M. Berg, "Feedback regularization and geometric PID control for trajectory tracking of mechanical systems: Hoop robots on an inclined plane," in *Proc. Amer. Control Conf. (ACC)*, Seattle, WA, USA, May 2017, pp. 3938–3943.
[20] T. Yu, H. X. Sun, Q. X. Jia, Y. H. Zhang, and W. Zhao, "Decoupled sliding mode control for the climbing motion of spherical mobile robots," in *Proc. Conf. Future Comput. Control Syst.*, Changsha, China, Apr. 2012, pp. 671–677.
[21] T. Yu, H. X. Sun, Q. X. Jia, Y. H. Zhang, and W. Zhao, "Sliding mode control of pendulum-driven spherical robots," *Adv. Mater. Res.*, vols. 591–593, pp. 1519–1522, Nov. 2012.
[22] M. Yue and B. Liu, "Adaptive control of an underactuated spherical robot with a dynamic stable equilibrium point using hierarchical sliding mode approach," *Int. J. Adapt. Control Signal Process.*, vol. 28, no. 6, pp. 523–535, Jun. 2014.
[23] S. Ladaci and A. Charef, "On fractional adaptive control," *Nonlinear Dyn.*, vol. 43, no. 4, pp. 365–378, Mar. 2006.
[24] Z. Ma, Z. H. Zhu, and G. Sun, "Fractional-order sliding mode control for deployment of tethered spacecraft system," *Proc. Inst. Mech. Eng. G, J. Aerosp. Eng.*, vol. 233, no. 13, pp. 4721–4734, Oct. 2019.
[25] T. Zhou, Y. G. Xu, and B. Wu, "Fractional order hierarchical sliding mode control of linear motion velocity of spherical robot," in *Proc. CCDC*, Chongqing, China, May 2017, pp. 7960–7964.
[26] T. Yu, K. Yang, and W. Zhao, "Adaptive robust trajectory tracking control of a spherical robot," *China Meas. Test*, vol. 44, no. 3, pp. 102–108, 2018.
[27] C. K. Shi, "Research on a spherical robot with manipulator used in emergency rescue," Ph.D. dissertation, Dept. Mech. Eng., Beijing Univ. Posts Telecommun., Beijing, China, 2010.
[28] M. Chu, "Research on the dynamics and active control strategies for space flexible manipulator," Ph.D. dissertation, Dept. Mech. Eng., Beijing Univ. Posts Telecommun., Beijing, China, 2010.
[29] M. Yue, B. Liu, C. An, and X. Sun, "Extended state observer-based adaptive hierarchical sliding mode control for longitudinal movement of a spherical robot," *Nonlinear Dyn.*, vol. 78, no. 2, pp. 1233–1244, Oct. 2014.
[30] Y. Y. Zhao, "Some theoretical properties and examples of the fractional calculus," M.S. thesis, Dept. Appl. Math., Zhengzhou Univ., Zhengzhou, China, 2013.
[31] Z. C. Xu, "Realization and department analysis of fractional-order controller based on LabVIEW," M.S. thesis, Dept. Control theor. Control Eng., Dalian Jiaotong Univ., Dalian, China, 2013.
[32] D. W. Qian and J. Q. Yi. *Hierarchical Sliding Mode Control for Under-actuated Cranes*. New York, NY, USA: Springer-Verlag, 2016, pp. 119–124.
[33] M. Zeinali and L. Notash, "Adaptive sliding mode control with uncertainty estimator for robot manipulators," *Mechanism Mach. Theory*, vol. 45, no. 1, pp. 80–90, Jan. 2010.
[34] M. Ö. Efe, "Integral sliding mode control of a quadrotor with fractional order reaching dynamics," *Trans. Inst. Meas. Control*, vol. 33, no. 8, pp. 985–1003, Dec. 2011.
[35] A. Dumlu, "Design of a fractional-order adaptive integral sliding mode controller for the trajectory tracking control of robot manipulators," *Proc. Inst. Mech. Eng. I, J. Syst. Control Eng.*, vol. 232, no. 9, pp. 1212–1229, Oct. 2018.
[36] C.-L. Hwang, H.-M. Wu, and W.-H. Hung, "Software/Hardware-based hierarchical finite-time sliding-mode control with input saturation for an omnidirectional autonomous mobile robot," *IEEE Access*, vol. 7, pp. 90254–90267, 2019.
[37] Y. Y. Min and Y. G. Liu, "Barbalat lemma and its application in analysis of system stability," *J. Shandong Univ.*, vol. 37, no. 1, pp. 51–55, 2007.

LONG MA received the B.S. and M.S. degrees in mechatronic engineering from the North University of China, Taiyuan, China, in 2012 and 2015, respectively. He is currently pursuing the Ph.D. degree in mechatronic engineering with the Beijing University of Posts and Telecommunications, Beijing, China.

His research topics include mechanism design, trajectory tracking control, and lateral slip control method of high-speed spherical robot.

HANXU SUN received the B.S. degree from the Shaanxi University of Technology, Xi'an, China, in 1982, the M.S. degree from the Chinese Academy of Sciences, Beijing, China, in 1986, and the Ph.D. degree from the Beijing University of Aeronautics and Astronautics, Beijing, China, in 1989.

He is currently a Professor with the School of Automation, Beijing University of Posts and Telecommunications. His research topics include spherical robotics, space robotics, pattern recognition, and human–robot collaboration.

JINGZHOU SONG (Member, IEEE) received the B.S. and M.S. degrees from the Changchun University of Science and Technology, Changchun, China, in 1998 and 2001, respectively, and the Ph.D. degree from the Beijing University of Aeronautics and Astronautics, Beijing, in 2006.

He is currently a Full Associate Professor with the Automation School, Beijing University of Posts and Telecommunications. His research topics include robot teleoperation, robot compliance control, haptic feedback interaction, human–robot collaboration, and reconfigurable sphere robot.